Thermodynamic and Experimental Investigation of Solar-Driven Biomass Pyro-Gasification Using H2O, CO2, or ZnO Oxidants for Clean Syngas and Metallurgical Zn Production

Srirat Chuayboon, Stéphane Abanades

processes

MDPI

Article

Thermodynamic and Experimental Investigation of Solar-Driven Biomass Pyro-Gasification Using H_2O, CO_2, or ZnO Oxidants for Clean Syngas and Metallurgical Zn Production

Srirat Chuayboon [1] and Stéphane Abanades [2,*]

[1] Department of Mechanical Engineering, King Mongkut's Institute of Technology Ladkrabang, Prince of Chumphon Campus, Chumphon 86160, Thailand; srirat.ch@kmitl.ac.th
[2] Processes, Materials and Solar Energy Laboratory, PROMES-CNRS, 7 Rue du Four Solaire, 66120 Font-Romeu, France
* Correspondence: stephane.abanades@promes.cnrs.fr; Tel.: +33-(0)4-68-30-77-30

Abstract: The solar gasification of biomass represents a promising avenue in which both renewable solar and biomass energy can be utilized in a single process to produce synthesis gas. The type of oxidant plays a key role in solar-driven biomass gasification performance. In this study, solar gasification of beech wood biomass with different oxidants was thermodynamically and experimentally investigated in a 1.5 kW_{th} continuously-fed consuming bed solar reactor at 1200 °C under atmospheric pressure. Gaseous (H_2O and CO_2) as well as solid (ZnO) oxidants in pellet and particle shapes were utilized for gasifying beech wood, and the results were compared with pyrolysis (no oxidant). As a result, thermodynamic predictions provided insights into chemical gasification reactions against oxidants, which can support experimental results. Compared to pyrolysis, using oxidants significantly promoted syngas yield and energy upgrade factor. The highest total syngas yield (63.8 mmol/$g_{biomass}$) was obtained from biomass gasification with H_2O, followed by CO_2, ZnO/biomass mixture (pellets and particles), and pyrolysis. An energy upgrade factor (U) exceeding one was achieved whatever the oxidants, with the maximum U value of 1.09 from biomass gasification with ZnO, thus highlighting successful solar energy storage into chemical products. ZnO/biomass pellets exhibited greater gas yield, particularly CO, thanks to enhanced solid–solid reaction. Solid product characterization revealed that ZnO can be reduced to high-purity Zn through solar gasification, indicating that solar-driven biomass gasification with ZnO is a promising innovative process for CO_2-free sustainable co-production of metallic Zn and high-quality syngas.

Keywords: thermochemical conversion; biomass; chemical looping gasification; solar reactor; metal oxide; metallurgy

Citation: Chuayboon, S.; Abanades, S. Thermodynamic and Experimental Investigation of Solar-Driven Biomass Pyro-Gasification Using H_2O, CO_2, or ZnO Oxidants for Clean Syngas and Metallurgical Zn Production. *Processes* **2021**, *9*, 687. https://doi.org/10.3390/pr9040687

Academic Editor: Axel Funke

Received: 29 March 2021
Accepted: 12 April 2021
Published: 14 April 2021

1. Introduction

Due to the concerns related to diminution of fossil fuels reserves and rise of greenhouse gas emissions, renewable energy sources have been increasingly used to replace fossil fuels. The leading renewable energy sources consist of solar, biomass, hydropower, wind, and geothermal. Noticeably, renewable biomass and solar resources can be integrated within a solar gasification process [1]. The solar gasification process represents a promising avenue to convert solid carbonaceous materials into green synthesis gas (H_2 + CO) [2]. With this process, intermittent solar energy can be long-term stored into dispatchable chemical products through enthalpy of endothermic reactions.

Conventional gasification technologies, originated over several decades, exhibit a major serious concern regarding the partial combustion of feedstock up 45% to drive endothermic chemical reactions [3]. In contrast, solar gasification has the potential to totally convert biomass to syngas thanks to the use of solar energy supplied as an external

heat source (allothermal), thereby outperforming the conventional autothermal route. However, it faces challenging issues involving intermittency (day and night cycle) and fluctuations due to variable weather conditions. To cope with these limitations, hybrid solar-autothermal gasification has been investigated [4]. Solar gasification performance depends on several key aspects involving reactor designs, temperatures, starting solid carbonaceous materials, reactants feeding rates, and types of oxidant [5].

Solar gasification reactors have been intensively designed, fabricated, and tested, including, e.g., packed bed reactors [6], fluidized bed reactors [7], vortex and entrained flow reactors [8]. Packed bed reactors [9] provide long residence time, which promotes feedstock conversion efficiency. However, their major drawbacks are high temperature gradients, heat and mass transfer limitations, and potentially discontinuous operation. To alleviate such issues, fluidized bed reactors were investigated [7]. However, constraints also exist regarding limited biomass particle size, and reactors could not be operated in continuous mode. Vortex and entrained flow reactors were designed to perform the process continuously, whilst maiming residence time. In addition, they still also face an issue of feedstock size limitation [10].

Recently, a research work at PROMES-CNRS laboratory aimed to design, fabricate, and test an original continuous spouted-bed solar gasification reactor [11]. This reactor both allowed for continuous operation and heat and mass transfer improvement, and it provided long solid residence time [12].

The gasification process starts with the removal of moisture at above 100 °C. It is then followed by pyrolysis in which biomass devolatilizes to biochar, incondensable gases (mainly H_2, CO, CO_2, H_2O, C_2H_2, C_2H_6), and tars at above 300 °C, according to Equation (1):

$$\text{Biomass} \rightarrow \text{biochar (carbon)} + CO + CO_2 + H_2 + H_2O + CH_4 + C_2H_2 + C_2H_6 + \text{tars} \quad (1)$$

Afterward, the produced biochar from pyrolysis is oxidized with the added gasification agents at above 800 °C. The ideal stoichiometric gasification reaction of beech wood biomass (with empirical chemical formula $C_6H_9O_4$) with water steam (Equation (2)) and CO_2 (Equation (3)) proceeds as follow:

$$C_6H_9O_4 + 2H_2O \rightarrow 6.5H_2 + 6CO \quad (2)$$

$$C_6H_9O_4 + 2CO_2 \rightarrow 4.5H_2 + 8CO \quad (3)$$

Alternatively, the gasification reaction with solid oxidants is possible [13]. Solid ZnO oxidant represents a favorable candidate for solar biomass gasification because its reduction temperate with carbonaceous materials is moderate (as compared to the thermal dissociation of ZnO ($ZnO \leftrightarrow Zn + \frac{1}{2}O_2$) which requires temperatures above 1500 °C [14]), and it suitably matches the gasification temperature [15].

Stoichiometric beech wood biomass gasification reaction with solid ZnO (Equation (4)) may be written as follow:

$$C_6H_9O_4 + 2ZnO \rightarrow 2Zn + 6CO + 4.5H_2 \quad (4)$$

During reaction (Equation (4)) taking place, the following side reactions, associated with the presence of ZnO, are possible:

$$ZnO + C \rightarrow Zn + CO \quad (5)$$

$$ZnO + CO \leftrightarrow Zn + CO_2 \quad (6)$$

$$ZnO + H_2 \leftrightarrow Zn + H_2O \quad (7)$$

Other possible secondary reactions occurring during the gasification process are associated with solid-gas and gas phase reactions:

$$C + CO_2 \leftrightarrow 2CO \quad (8)$$

$$C + H_2O \rightarrow CO + H_2 \quad (9)$$

$$CO_2 + H_2 \leftrightarrow CO + H_2O \quad (10)$$

$$CH_4 + CO_2 \rightarrow 2CO + 2H_2 \quad (11)$$

$$CH_4 + H_2O \rightarrow CO + 3H_2 \quad (12)$$

This ZnO reduction process using biomass as reducer allows operating at much lower temperature than that required for the solar thermal reduction process ($ZnO \rightarrow Zn(g) + \frac{1}{2}O_2$), as part of the two-step ZnO/Zn redox cycle for H_2O and CO_2 splitting [16,17]. The produced solid Zn derived from solar thermochemical conversion process can be recycled to ZnO after reacting with H_2O (Equation (13)) or CO_2 (Equation (14)) to produce H_2 or CO in a two-step cycle [18,19]:

$$Zn + H_2O \rightarrow ZnO + H_2 \quad (13)$$

$$Zn + CO_2 \rightarrow ZnO + CO \quad (14)$$

Solar-driven gasification with gaseous or solid oxidants was previously investigated numerically [20], experimentally [21], and economically [22]. Concerning solid oxidants, Bellouard et al. [23] employed iron oxide to gasify beech wood biomass and found that iron oxide was reduced to metallic iron, depending on the oxygen carrier proportion. They also concluded that iron oxide is an effective candidate for producing both syngas and iron via a novel green metallurgical process. Chuayboon et al. [15] reported that ZnO can oxidize biomass, and biomass/ZnO ratios have an important impact on gasification performance. In addition, Yang et al. [24] studied chemical looping gasification using Fe supported on phosphogypsum compound as an oxygen carrier, and reported that this material has high oxygen exchange capacity, high selective conversion ability of C to CO, excellent activity and recyclability. Furthermore, the effect of equivalence ratio on the CO selectivity of Fe/Ca-based oxygen carriers in biochar chemical looping gasification was investigated [25], and the CO selectivity of Fe_2O_3 decreased markedly with increasing equivalence ratio. Concerning gaseous oxidants, CO_2 and H_2O were mostly used for solar biomass gasification thanks to their physicochemical benefits [26,27]. Bellouard et al. [11] studied continuous solar biomass gasification with both CO_2 and H_2O in an innovative spouted-bed solar reactor. CO_2 gasification was found to exhibit lower kinetic rate compared to H_2O gasification.

According to previous studies, the oxidizing agents played a key role in solar biomass gasification. Therefore, this study aimed to thermodynamically and experimentally investigate the influence of oxidants including H_2O, CO_2, and ZnO on solar-driven biomass gasification in a continuously-fed consuming bed gasification reactor. The performance outputs of biomass gasification with the different oxidizing agents were determined and further compared with pyrolysis (no oxidant). Syngas production rates, yields, and reactor performance metrics, as well as solid product characterizations, were evaluated to demonstrate the effect of oxidant type on the gasification process.

2. Materials and Methods

2.1. Reactants and Carbonaceous Feedstock

Beech wood biomass (empirical chemical formula $C_6H_9O_4$ obtained from elemental composition analysis) was employed as the renewable solid carbonaceous feedstock. Its physical and chemical properties are displayed in Table 1. ZnO was supplied as a solid oxidant, while H_2O and CO_2 were employed as gaseous oxidants. ZnO powder (99% purity, 1–5 μm particle size) was purchased from PROLABO (Paris, France). Research

grade CO_2 (99.999% purity) and high-purity distilled H_2O were utilized. Biomass particles and ZnO powder were mechanically mixed with an adequate ZnO content with respect to the stoichiometric mixture (Equation (4)). Given the different granulometry, the ZnO powder covered the biomass particles surface uniformly. In addition, H_2O and CO_2 were also fed to fulfil stoichiometric proportions (with respect to Equation (2) and Equation (3), respectively), so that the influence of the oxidants could be compared. Two types of biomass and ZnO mixture consisting of either particles blend or pressed pellets were prepared. Concerning the pellet morphology, it was prepared using a manual hydraulic press at a pressure of ~75 kg/cm^2 for 2 min/pellet, resulting in 0.471 cm^3/pellet volume and 10 mm diameter.

Table 1. Physical and chemical properties of beech wood biomass.

Elemental Chemical Composition						Moisture (wt%)	Volatile Matter (wt% db)	Fixed Carbon (wt% db)	Mean Particle Sizeh (mm)	Apparent Densityh (g/cm^4)	LHV (MJ/kg)
C (wt% db)	H (wt% db)	O (wt% db)	N (wt% db)	S (wt% db)	Ash (wt% db)						
48.3	6.7	44.4	0.11	<0.1	0.46	8.9	83.3	15.2	1	0.201	18.3

2.2. Solar Reactor and Methods

Figure 1 displays the experimental set-up consisting of a 1.5 kW_{th} continuously-fed consuming bed reactor with its essential components. The solar reactor is cylindrical and mainly consists of a vertical high-temperature resistant alumina cavity receiver (wall thickness: 5 mm, 60 × 50 mm diameter, and 70 mm height). The cavity was insulated with a 30 mm-thick alumino-silicate porous ceramic layer, and its bottom was drilled to allow the passage of an inlet tube (4 × 2 mm) through which gaseous oxidants (H_2O or CO_2) were injected. The whole internal components were positioned within a water-cooled stainless-steel reactor shell. Reactor temperatures were measured by a B-type thermocouple, which was inserted in the cavity receiver and compared with measurement of a solar-blind pyrometer (operating at 4.8–5.2 μm), which was positioned at the center of the facedown parabolic dish concentrator (Figure 1). In addition, the reactor pressure was measured by a pressure transducer. Lastly, a hemispherical transparent glass window was fixed to the front flange edge of the reactor shell for gas-tightness experiments. The feedstock was fed in the form of particles (either biomass or biomass/ZnO mixture) via a reactant delivery system composed of a hopper, screw feeder, and electrical motor. Its tip was inserted through the inlet reactant injection port at the cavity lateral side. Besides, a manual pushing rod was used instead of the screw feeder for injecting reactant pellets (ZnO/biomass). Regardless of the feeding device, the reacting feedstock (either biomass or biomass/ZnO mixture) fell inside the cavity by gravity. A thin layer of alumina wool and particles was placed at the cavity bottom to support the fed reactant and to broaden the inlet gas stream (injected from the cavity bottom) to the whole cavity section.

The solar chemical reactor was installed at the focus of a 1.5 kW_{th} vertical-axis solar furnace of PROMES laboratory, Odeillo, France. Incident sunlight was reflected by a 2 m^2 automatic sun-tracking heliostat and subsequently concentrated by a 2 m-diameter solar dish concentrator, thereby providing highly concentrated sunlight (beyond 10 MW/m^2 of flux density with Gaussian distribution, for Direct Normal Irradiation (DNI) of 1000 W/m^2). Concentrated sunlight entered the cavity receiver through an alumina cap with a 15 mm diameter aperture to efficiently capture solar energy while minimizing radiative heat losses.

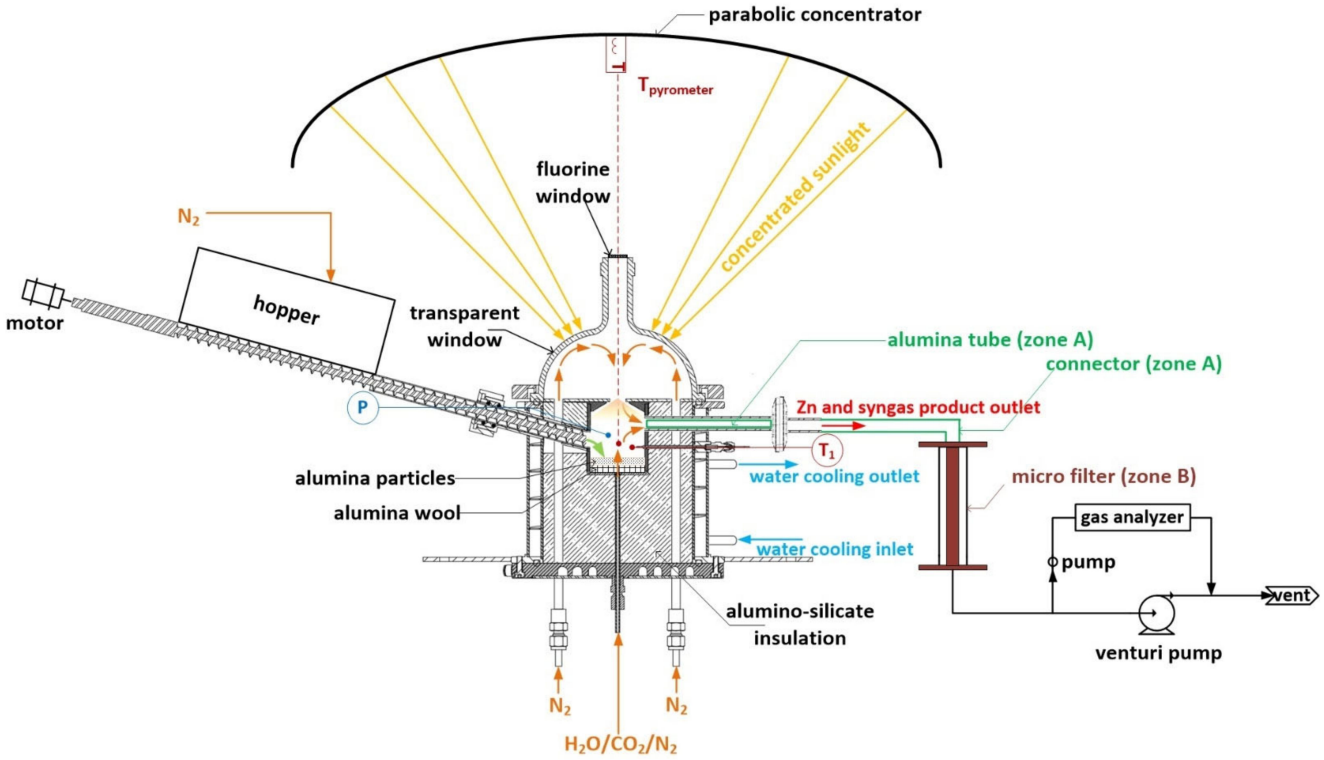

Figure 1. Schematic diagram of the 1.5 kW_{th} continuous biomass gasification reactor with its main external components (P = reactor cavity pressure and T_1 = reactor cavity temperature).

During heating, N_2 protective and N_2 carrier gases flowed to the transparent window and reactor cavity, and they exited through the lateral reactor outlet. Once reaching the targeted temperature, biomass and gaseous H_2O/CO_2 oxidants were initiated across their inlet ports to the reactor cavity in continuous injection mode. For solid oxidant, a mixture of biomass and solid ZnO oxidant was fed directly via the biomass injection port. Gasification reactions took place continuously till complete reactant injection. DNI was stable (1000 W/m^2) throughout on-sun experiments. Experiments were conducted at 1200 °C under atmospheric pressure of 0.90 bar (at the experimental site location). Gas product species involving syngas and Zn(g) exited the reactor via the outlet alumina tube (represented as zone A) and then went through a micro filter (represented as zone B). Zn was condensed when the gas stream exited the cavity, and was recovered in the form of solid deposits in both the outlet alumina tube and the filter. A fixed flow rate of product gases was sampled for continuous gas analysis (Emerson X-STREAM XEGP, St. Louis, MO, USA), using infrared detectors for CO, CO_2, CH_4 and thermal conductivity detector for H_2 (uncertainty < 0.5% of full scale). Punctual gas analysis (every 2–3 min) was also performed by gas chromatography (Varian CP4900, Palo Alto, USA) to validate gas concentration measurements. In case of steam gasification, the outlet gas flowed through a gas drying unit (bubbler) to remove unconverted steam and a filter to remove entrained particles, before gas composition analysis. In addition, the outlet amounts of H_2O (condensed in the outlet components) and entrained char were quantified by weighting for mass balance validation whatever the type of oxidizing agent (H_2O, CO_2, and ZnO).

In case of biomass gasification with ZnO, the produced Zn vapor that was condensed mainly at the outlet alumina tube (zone A), followed by the micro filter (zone B) was collected for characterization. They were sampled and analyzed by X-ray diffraction (XRD) for phase identification (Philips PW 1820 diffractometer, Amsterdam, Netherlands) using the Cu Kα radiation (αCu = 1.5418 Å, angular range = 20–100° in 2-Theta, step size of 0.02°, recording time = 2 s), and by field emission scanning electron microscopy (FESEM, Hitachi S4800, Tokyo, Japan) for morphology analysis.

The solar reactor performance indicators were determined including the syngas yields and energy upgrade factor. The energy upgrade factor (U) represents the ratio of the energy content of the chemical products to the calorific value of the biomass feedstock (Equation (15)). In case of beech wood gasification with CO_2/H_2O, only the syngas calorific value was taken into account, whereas both syngas and zinc calorific values were included for biomass gasification combined with ZnO reduction. In fact, U quantifies the fraction of solar energy stored in the reaction products. The U value is higher than 1 when the energy content of the products is higher than that of the feedstock, meaning that solar energy has been effectively stored in the reaction products. Note that the energy content of the char by-product remaining in the cavity (especially in the case of pyrolysis) was not taken into account in the calculation, which resulted in low U value.

$$U = \frac{\left(LHV_{syngas}\dot{m}_{syngas}\right) + \left(\dot{n}_{Zn}\Delta H_{Zn+0.5O_2\rightarrow ZnO}\right)}{LHV_{feedstock}\dot{m}_{feedstock}} \quad (15)$$

3. Results and Discussion

3.1. Thermodynamic Equilibrium Analysis

Thermodynamic equilibrium was studied utilizing a Gibbs free energy minimization approach (HSC chemistry) for a closed system, in which kinetic limitations are not considered (thus assuming residence times are high enough to reach equilibrium). The purpose of the thermodynamic equilibrium analysis is to provide insights into the products distribution for each reaction involving pyrolysis and gasification with gaseous H_2O/CO_2 and solid ZnO oxidants, as a function of the temperature. The equilibrium approach provides support to the experiments regarding the chemical reaction mechanism (as a function of the temperature and oxidant type), the required temperature for reaction completion, and the equilibrium gas composition. It was thus employed as a first approach to determine the theoretical limit of the thermochemical conversion process and to identify the expected products. Figure 2 shows the equilibrium product distribution as a function of temperature for beech wood biomass pyrolysis at 1 bar. Higher hydrocarbons (C_nH_m) were taken into account in the calculation; however, their amounts were found to be negligible and were thus omitted.

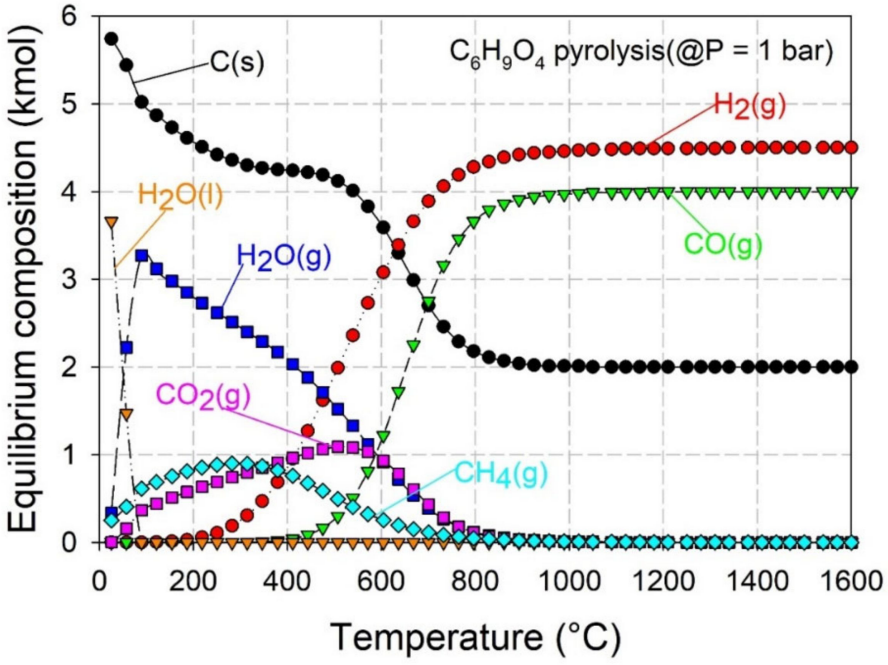

Figure 2. Thermodynamic equilibrium products distribution of biomass pyrolysis (1 kmol of $C_6H_9O_4$) at 1 bar.

As a result, in the initial state, moisture (H_2O(l)) contained in the biomass, first vaporized to H_2O(g), and then biomass thermally decomposed to C(s), CO_2, CH_4, and H_2 in the absence of oxygen (Equation (1)). At below 400 °C, CH_4 and CO_2 were predominant compared to CO and H_2. With increasing temperature, CH_4 and CO_2 decreased while H_2 and CO increased. The reaction approached and then reached completion at above 800 and 1000 °C, respectively (as reflected by a stable products composition above 1000 °C), resulting in a gas phase including CO and H_2 and a solid phase involving biochar with a CO(g)/C(s) ratio of two (pyrolysis reaction can be written as: $C_6H_9O_4 \rightarrow 2C_{(s)} + 4CO + 4.5H_2$).

Thermodynamic equilibrium compositions of biomass gasification with H_2O and CO_2 (Equations (2) and (3)) as a function of temperature at 1 bar are presented in Figures 3 and 4, respectively. They were calculated under stoichiometric mixture. As observed in Figure 3 (H_2O gasification), at the initial state, biomass decomposition was enhanced when compared with pyrolysis (Figure 2) thanks to the H_2O oxidant, as evidenced by a steep decline in C(s). Similar to pyrolysis, CO_2 and CH_4 decreased with increasing temperature. The reaction reached completion above 900 °C, resulting in a stoichiometric mixture of a gas phase consisting of H_2 (6.5 mol) and CO (6 mol), without the presence of solid carbon.

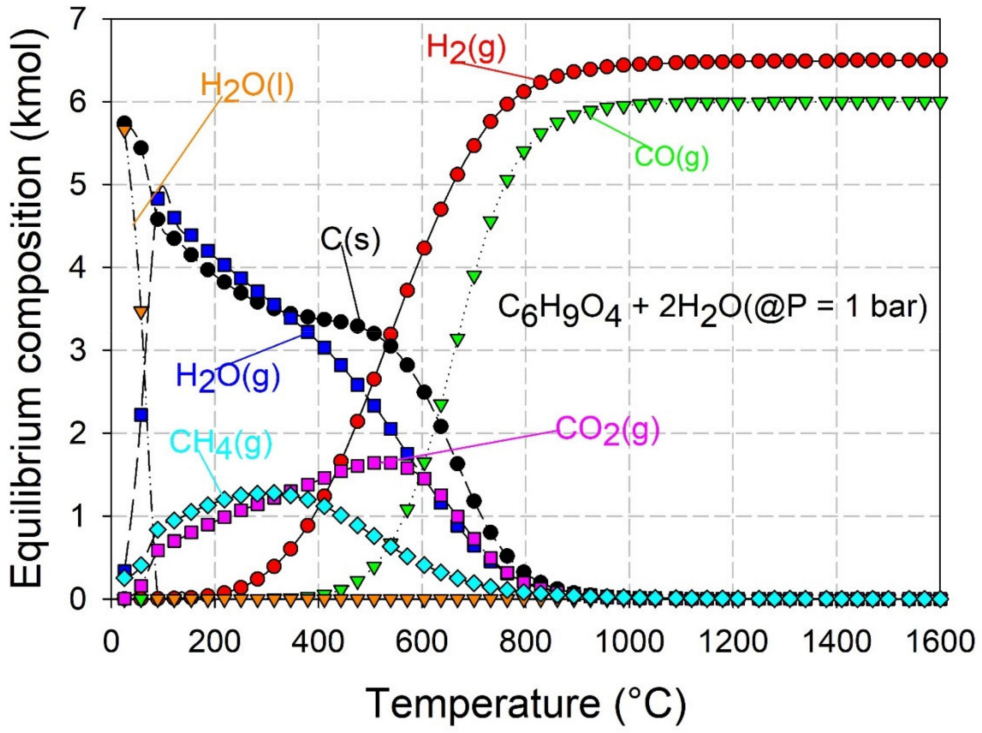

Figure 3. Thermodynamic equilibrium products distribution of the biomass steam gasification ($C_6H_9O_4 + 2H_2O$) system at 1 bar.

Regarding CO_2 gasification (Figure 4), in the initial state, H_2 and CH_4 were formed in lower amounts, whereas CO was higher compared to steam gasification (Figure 3). As expected, employing CO_2 as an oxidant resulted in higher CO production than using H_2O (8 mol of CO and 4.5 mol of H_2 at above 1000 °C). Moreover, it decreased H_2 production. The stoichiometric mixture of H_2 and CO (given by Equation (3)) was reached above 1000 °C, which denotes reaction completion, as evidenced by a stable pattern of the gas composition versus temperature. The temperature for reaction completion was slightly higher than for H_2O gasification (above 1000 °C (CO_2) vs. above 900 °C (H_2O)). This is because of the Boudouard equilibrium (Equation (8)) that requires a higher temperature for reaction completion [23], which translates into much slower kinetics compared to carbon gasification with H_2O (Equation (9)) [28].

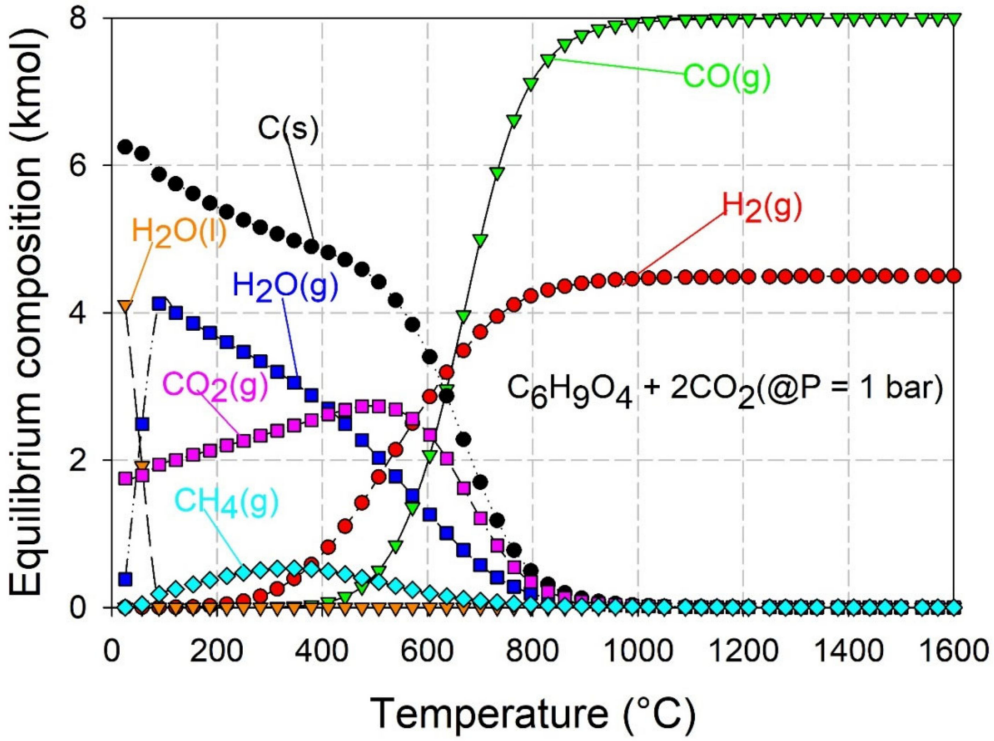

Figure 4. Thermodynamic equilibrium products distribution of the biomass dry gasification ($C_6H_9O_4$ + $2CO_2$) system at 1 bar.

Figure 5 shows thermodynamic equilibrium composition of biomass gasification with solid ZnO oxidant (Equation (4)) as a function of temperature at 1 bar. In agreement with pyrolytic process (Figure 2), in the initial state, biomass was thermally decomposed to incondensable gases (Equation (1)), while ZnO was thermodynamically stable up to ~800 °C. Between 800 °C and 900 °C, ZnO(s) was reduced to Zn in both liquid and gaseous phases. In the meantime, the char produced from pyrolysis was oxidized with ZnO (Equation (5)), CO_2 (Equation (8)), and H_2O (Equation (9)). The reactions according to Equations (6), (7) and (10)–(12) could concomitantly take place. The reaction approached and then reached completion at above 800 °C and above 1000 °C, respectively, similar to CO_2 gasification. The final main products were a gas phase consisting of Zn vapor (2 mol), CO (6 mol), and H_2 (4.5 mol) with an H_2/CO ratio of 0.75. In contrast to pyrolysis, C(s) was totally converted to CO at above 1000 °C. In summary, the absence of oxidant (pyrolysis reaction) resulted in char remaining in addition to the produced syngas at thermodynamic equilibrium above ~800 °C. Employing H_2O or CO_2 oxidant led to syngas production, while using ZnO oxidant led to both syngas and metallic Zn. The reported mechanisms and products distribution were predicted by thermodynamic equilibrium. Because kinetic limitations can modify the equilibrium composition, experimental study is needed to assess the real products formation at the given operating conditions.

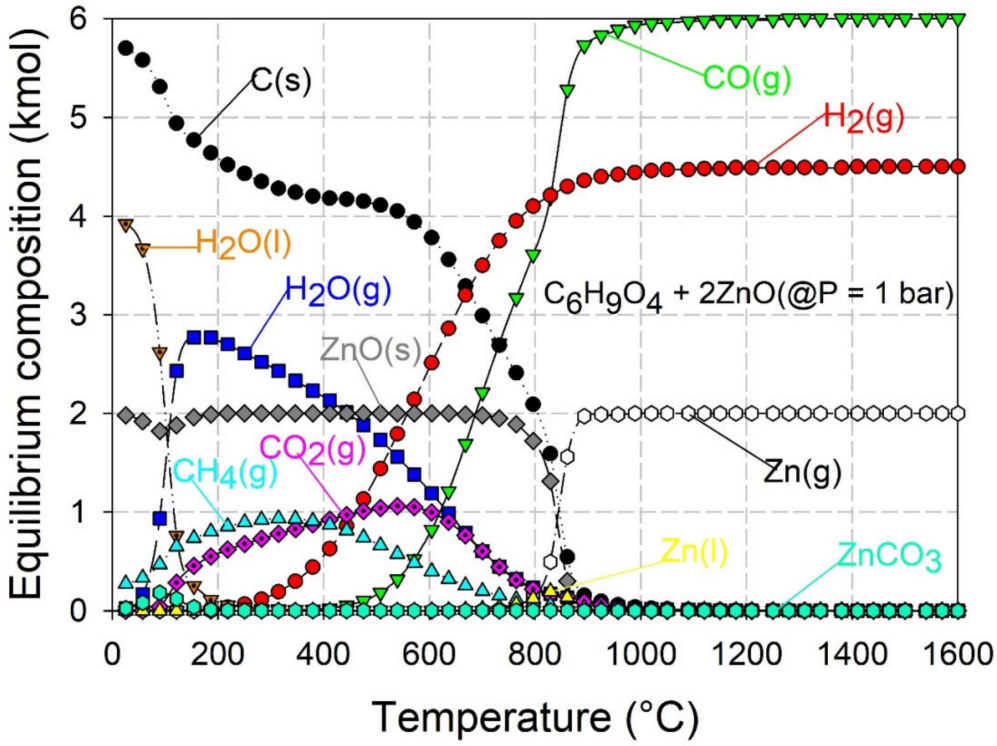

Figure 5. Thermodynamic equilibrium products distribution of the biomass gasification with ZnO ($C_6H_9O_4$ + 2ZnO) system at 1 bar.

3.2. Representative Solar Gasification Experiment

Figure 6 shows the syngas production rates consisting of CO, CO_2, CH_4, H_2, and C_nH_m and reactor temperature T_1 (right) during continuous solar beech wood gasification with H_2O at 1200 °C. Wood biomass (30 g) was injected at ~1.1 g/min while H_2O was introduced at 0.2 g/min, resulting in a slight excess of H_2O (in order to favor biomass conversion to syngas [29]). Overall, a continuous biomass gasification reaction was accomplished within ~27–30 min duration with high H_2 and CO production rates exceeding 0.9 NL/min. During the first 20 min, H_2/CO ratio was found to be stable around 1.2–1.4 (and afterward fluctuated in the range 0.6–1.8). A fluctuation in the syngas production rate over time provides insight into the biomass injection instability, presumably due to the irregular shape and size of the biomass. This experiment was achieved during suitable solar irradiation conditions with average DNI around 1000 W/m^2, and the resulting temperature evolution was thus stable around 1200 °C. After 20 min duration, the syngas dropped drastically due to a stop in the biomass feed rate resulting from a temporal feeding blockage. Such transient reactant feeding blockage, encountered during injection, could be circumvented by inducing mechanical vibration on the reactant feeding delivery system. The gas production rates then rose again and finally reached zero after complete injection of the biomass load. In comparison, the syngas production rates determined by online analysis (solid lines) were consistent with those obtained from online gas chromatography (dot lines), thus confirming results reliability. The syngas yields (millimole per gram of dry biomass, mmol/$g_{biomass}$) were then calculated by time integration of the gas production rates over the experiment duration. The reactor exhibited remarkable performance with production of a high-quality and energy-rich syngas. The global syngas yields reached 32.3 (H_2), 26.5 (CO), 2.8 (CH_4), 2.1 (CO_2), and 0.1 (C_2H_m) mmol/$g_{biomass}$, resulting in an average H_2/CO ratio of 1.2 over the experiment duration. Biomass conversion into syngas up to 82% and global mass balance up to 95% were achieved. The energy upgrade factor (U), defined as the energy contained in the produced syngas to that contained in the

biomass feedstock (Equation (15)), exceeded one, demonstrating solar energy storage into chemical products.

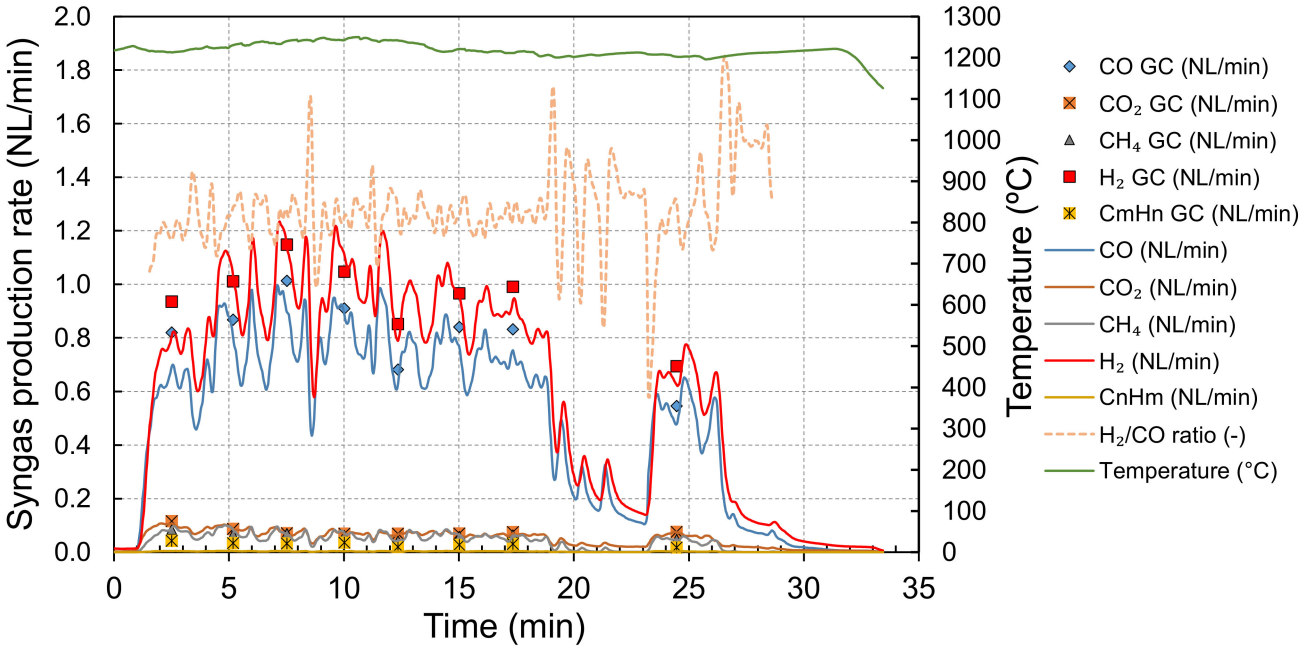

Figure 6. Representative experiment of solar beech wood gasification with H_2O (biomass amount = 30g, biomass feeding rate = 1.1 g/min, H_2O feeding rate = 0.2 g/min, temperature = 1200 °C).

3.3. Impact of Oxidant

ZnO, CO_2, and H_2O were individually supplied as oxidant in separate runs for gasifying beech wood biomass. The effect of the type of oxidant (either solid or gaseous) was thus studied. Experiments with continuous reactants injection were conducted at 1200 °C (nominal temperature T_1 inside the reactor cavity). Biomass particles (mass of 30 g) were injected at 1.1 g/min, while each of the oxidants was fed to comply with the reaction stoichiometry. Concerning biomass gasification with ZnO, two types of reactant injection (mixture of biomass and ZnO) were considered including pellets and particles blend, to unravel the effect of reactants mixing on solid-solid reaction. The particle delivery system was also used to feed the biomass/ZnO particles blend. Regarding pressed pellets, fifteen pellets of biomass + 2ZnO were loaded into the alumina feeding tube equipped with a pushing rod to inject the pellets individually via the injection port of the reactor.

The impact of ZnO (pellets or particles), CO_2, and H_2O oxidant on syngas yields was experimentally examined and compared with the yields of the pyrolysis process. Figure 7 displays the syngas yields along with the energy upgrade factor (U) of biomass pyrolysis and biomass gasification with ZnO (either particles or pellets), CO_2, and H_2O oxidants. The total syngas yield of each species including H_2, CO, CO_2, CH_4, C_nH_m (Figure 7) was obtained from time integration of the syngas production rates. The theoretical U values of 1.23 for H_2O + biomass (Equation (2)), 1.26 for CO_2 + biomass (Equation (3)), 1.31 for ZnO + biomass (Equation (4)), and 1.11 for biomass pyrolysis were also presented as reference values. For biomass + ZnO, the calorific value of produced Zn was also taken into account (in addition to syngas) to calculate U values. Noticeably, when accounting for the calorific value of C_2H_m measured from GC analysis, the U values, designated as $U(C_2H_m)$, were increased by 6%–10%.

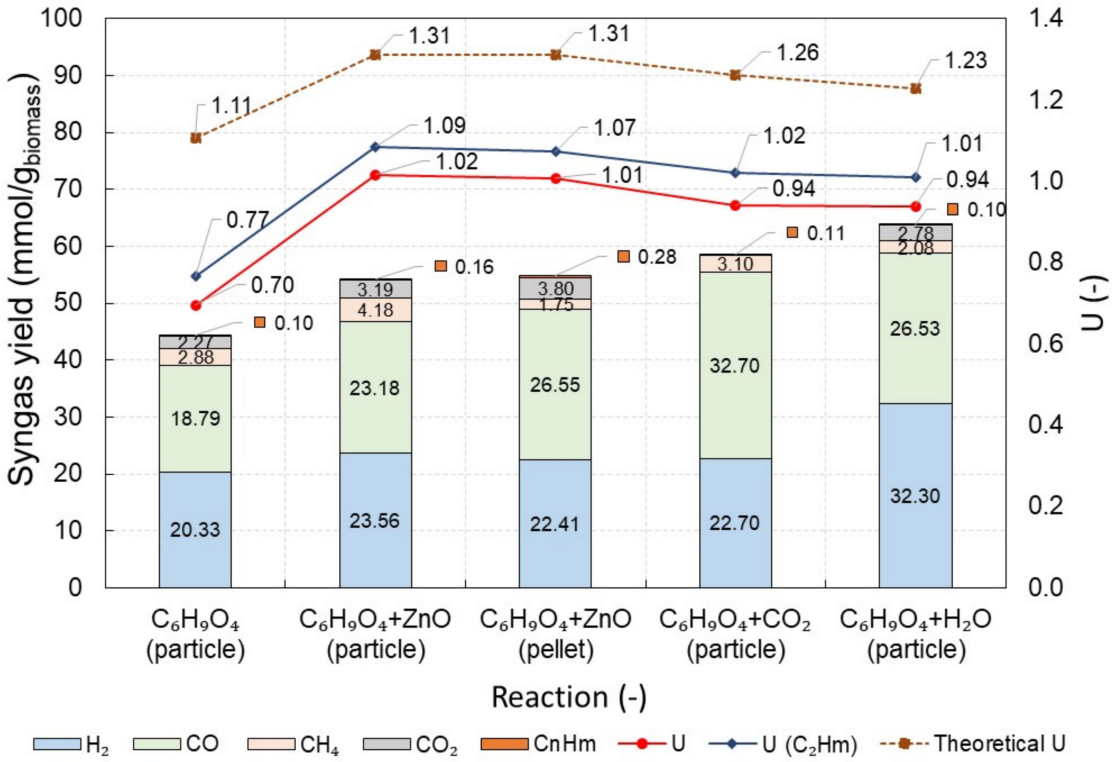

Figure 7. Syngas yields and energy upgrade factors (U) obtained from pyrolysis and gasification of biomass with ZnO, CO_2, and H_2O.

As a result, the impact of the type of oxidant on syngas yields was clearly evidenced, as reflected by the change in syngas yields as a function of the oxidant. The highest total syngas yield was reached from biomass + H_2O (63.8 mmol/$g_{biomass}$), followed by biomass + CO_2 (58.6 mmol/$g_{biomass}$), biomass + ZnO (pellets) (54.8 mmol/$g_{biomass}$), biomass + ZnO (particles) (54.3 mmol/$g_{biomass}$), and biomass pyrolysis (44.4 mmol/$g_{biomass}$). C_nH_m formation was found to be negligible for all tests. Note that in the case of CO_2 used as oxidant, the CO_2 produced by the gasification reaction in Figure 7 was not presented (because it was mixed with the unreacted CO_2). Compared to pyrolysis, using solid or gaseous oxidants enhanced both syngas yields and U, thanks to enhanced carbon conversion, in agreement with thermodynamic predictions. Experimental U(C_2H_m) values were above one whatever the oxidants, thus demonstrating successful solar energy storage into chemical products. In addition, they were higher than that of pyrolysis (below one in this case since not including the heating value of char), pointing out the advantages of using oxidants for enhancing the products energy content. The highest U(C_2H_m) was found for ZnO + biomass particles (1.09), followed by ZnO + biomass pellets (1.07), CO_2 + biomass (1.02), and H_2O + biomass (1.01). The experimental U(C_2H_m) values from ZnO + biomass were higher than those from CO_2 + biomass and H_2O + biomass, pointing out the benefit of using solid ZnO oxidant. This means that the energy content of the feedstock was upgraded by the solar power input in the form of both syngas and Zn, thus outperforming pyrolysis in addition to delivering higher syngas output per unit of feedstock.

Regarding gaseous oxidants (CO_2 vs. H_2O), the CO yield from CO_2 gasification was much higher while the H_2 yield was much lower, compared to H_2O gasification, in line with thermodynamic equilibrium predictions. This thus led to lower H_2/CO ratios (0.7 (CO_2) vs. 1.2 (H_2O)), corresponding to same tendencies of thermodynamic analysis. The CH_4 yield derived from CO_2 gasification was higher, because CH_4 + CO_2 dry reforming reaction (Equation (11)) is less favorable, compared to CH_4 + H_2O steam reforming (Equation (12)) at the given process temperature. Despite producing lower total syngas, the calculated

U(C_2Hm) from CO_2 gasification was found to be similar compared to H_2O gasification, due to higher amounts of CO and CH_4 which have high heating values.

Regarding solid oxidants (biomass/ZnO particles vs. biomass/ZnO pellets), the total syngas yield from biomass/ZnO pellets was slightly higher (54.8 mmol/$g_{biomass}$ (pellets) vs. 54.3 mmol/$g_{biomass}$ (particles)). The yields of H_2, CO, CH_4, and CO_2 were 23.56, 23.18, 4.18, and 3.19 mmol/$g_{biomass}$ for biomass/ZnO particles compared to 22.41, 26.55, 1.75, and 3.80 mmol/$g_{biomass}$ for pellets. Remarkably, the CO yield from biomass/ZnO pellets was significantly higher, pointing out the beneficial effect of pellet shape on gas yield. This behavior can be ascribed to the pellet compaction that promotes solid-solid reactions, in particular the reaction of ZnO with char producing CO (Equation (5)). However, the obtained value of U from biomass/ZnO pellets was lower owing to a lower amount of CH_4.

In summary, the presence of oxidant was proved to be important for converting biomass to syngas via solar gasification. On the one hand, if focusing on syngas yield, gaseous oxidants (CO_2 and H_2O) were more favorable than solid oxidants. On the other hand, using ZnO oxidant provided a promising opportunity to produce both syngas and metallic Zn at moderate temperature (easy to handle at large-scale) in a single process. In comparison to biomass/ZnO particles, pellets shape exhibited greater performance as evidenced by higher CO yield. Solar biomass pyrolysis is not properly adapted for biomass-to-syngas conversion; however, it can be an alternative option for co-production of syngas and solid carbon.

3.4. Solid Product Characterization

The production of metallic Zn powder from biomass gasification with ZnO (pellets and particles) was characterized. As illustrated in Figure 1, the outlet components were divided into two zones: (i) zone A is the outlet alumina tube and connector; and (ii) zone B is the micro filter. Accordingly, the solid products collected from both zones were characterized by X-ray diffraction (XRD) for identifying the ultimate phase (products quality) from diffraction data. Field emission scanning electron microscopy (FESEM) was performed for analyzing product morphology. XRD patterns of the solid products from biomass + ZnO (pellets) and biomass + ZnO (particles) gasification at 1200 °C under atmospheric pressure (0.90 bar) are presented in Figure 8. The results were compared with pure commercial Zn (pure Zn diffractogram) as reference pattern.

Overall, diffraction peaks of the Zn pattern were found to be clearly-defined and had high intensity for both zone A and zone B, whatever pellets or particles. This revealed that high-purity Zn was produced via the biomass gasification process. There was no effect of the reactant shape on solid product purity. Nevertheless, a small trace of remaining ZnO was evidenced in the cavity after solar experiments (Figure 8a), resulting from a slight excess of unreacted ZnO (this ZnO is not ascribed to Zn oxidation with CO_2 or H_2O because this reaction is not favorable at the high cavity temperature). At zone A (Figure 8b), the presence of ZnO was still detected, but in negligible amount for both particles and pellets injection. This weak ZnO formation may result from Zn recombination with CO (Equation (5) (reverse reaction)), and oxidation with CO_2 (Equation (13)) and H_2O (Equation (14)) that are thermodynamically favorable at low temperatures (during cooling in the outlet path). In contrast to zone A, only the Zn pattern was noticed at zone B for both particle and pellet reactant injection (Figure 8c), demonstrating no ZnO contamination and high-purity Zn production. Using Scherrer's equation, the mean crystallite size of the solid Zn products was found to be 40–80 nm for zone A and 40–60 nm for zone B.

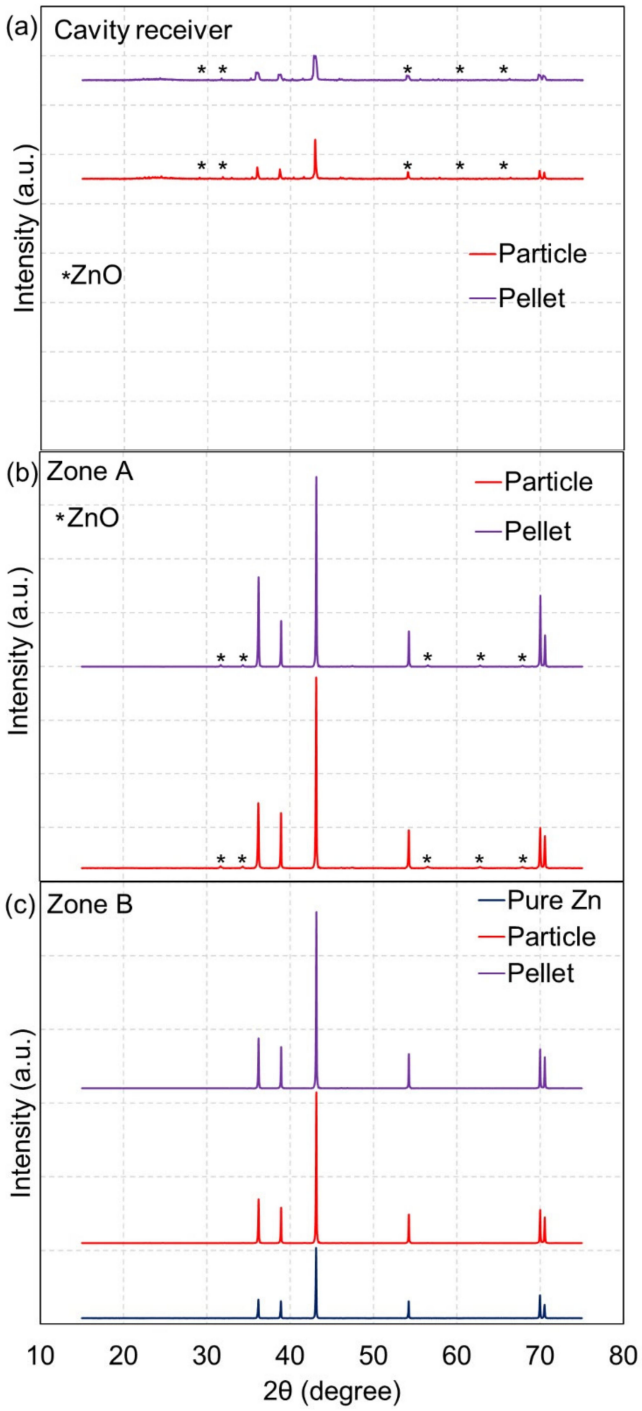

Figure 8. Representative X-ray diffraction (XRD) patterns of solid products from beech wood biomass gasification with ZnO in the form of particles and pellets: (**a**) solid product remaining in the cavity, (**b**) powder collected in zone A, and (**c**) powder collected in zone B.

Figure 9 shows FESEM micrographs of the remaining solid product in the cavity receiver (a), solid products collected in the reactor outlet (zone A, (b)), and in the micro filter (zone B, (c)), during biomass gasification with ZnO (with particles injection). Overall, Zn products were found in the form of submicronic grains and they were covered with dispersed biochar. The microstructure of remaining biochar in the cavity was mainly observed (Figure 9a), including some small amounts of remaining ZnO (ZnO remaining in the cavity receiver can be reused in subsequent solar gasification reactions). Interestingly, at zone A (Figure 9b) some of the Zn products grew in filaments (0.1–0.2 μm diameter),

and a part grew in plane layers resulting from the Zn product deposit in contact with the inner surface of the outlet water-cooled tube. At zone B (Figure 9c), condensed Zn in the form of scattered hexagonal grains was also observed, including fine biochar particles.

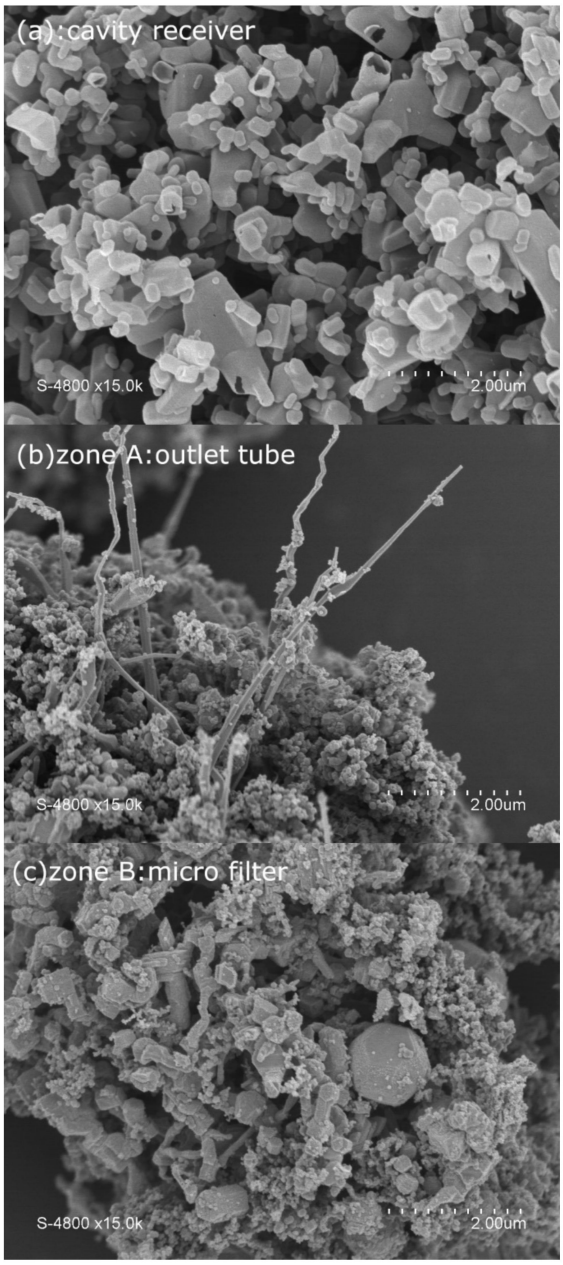

Figure 9. Field emission scanning electron microscopy (FESEM) micrographs of solid products collected in (**a**) the cavity, (**b**) the outlet tube and connector (zone A), and (**c**) the micro filter (zone B).

4. Conclusions

On-sun continuous solar pyrolysis and gasification of renewable beech wood biomass with different oxidizing agents have been successfully investigated. Experiments were carried out in a 1.5 kW_{th} continuously-fed consuming bed solar chemical reactor. Highly concentrated sunlight was utilized to drive chemical reactions, unveiling a promising means to store intermittent solar energy in the form of chemical products (solar fuels). H_2O or CO_2 were employed as gaseous oxidants for producing high-quality syngas, whereas ZnO was employed as solid oxidant for the co-production of green metallic Zn and syngas in a single sustainable process. The influence of oxidants on syngas yield and energy

upgrade factor (U) was underlined. In addition, thermodynamic equilibrium analysis was performed to highlight the effect of oxidant on gasification products distribution. Several key outcomes of this study can be outlined as follows:

- The thermodynamic analysis first provided essential understanding of the involved chemical reaction mechanism as a function of the temperature. Furthermore, the equilibrium species distribution was strongly dependent on the type of oxidant.
- A representative solar experiment demonstrated remarkable performance for the continuous solar-driven biomass gasification performed in a consuming-bed reactor, enabling high syngas production rates with small amounts of undesired by-products (CH_4, CO_2, and C_nH_m). The continuous solar reactor was further proved to be compatible with various oxidants for biomass gasification.
- The comparison of oxidants impact on reactor performance provided noteworthy outcomes. The gasification process employing oxidants, whether solid or gaseous, outperformed the pyrolysis process, which led to enhanced syngas yield and upgraded U.
- The interest of using gaseous H_2O and solid ZnO oxidants was highlighted, since the highest total syngas yield of 63.8 mmol/$g_{biomass}$ was reached from gasification with H_2O, and the highest U of 1.09 was achieved from gasification with ZnO. Utilizing CO_2 also exhibited great performance, with total syngas yield of 58.61 mmol/$g_{biomass}$ and increased CO formation at the expense of lowered H_2, in agreement with thermodynamic prediction.
- Using gaseous oxidants globally resulted in a simple handling system. ZnO solid oxidant was successfully reduced to Zn with syngas co-product during biomass gasification. Pellet reactants obtained by compaction exhibited higher gas yield, particularly CO, thanks to improved solid-solid reaction.
- High-purity Zn particles with crystallized hexagonal microstructure were produced from biomass gasification with ZnO. The Zn produced could be utilized in a Zn battery and further used as an oxygen carrier in a two-step CO_2/H_2O splitting system.
- Solar pyrolysis, although not optimal for producing syngas, can be an attractive pathway for producing both biochar and syngas.
- The various possible options in solid and gaseous oxidants make the gasification process flexible depending on the targeted products. In particular, the novelty of continuous solar gasification of biomass with solid oxidants represents a cutting-edge pathway toward renewable synthetic fuels and green metallurgical products.

Author Contributions: S.C. and S.A. created the ideas and research design of this paper; S.C. performed data analysis; S.C. and S.A. acquired the data; S.C. wrote the original draft; S.A. reviewed and edited the paper. All authors have read and agreed to the published version of the manuscript.

Funding: This research received no external funding.

Institutional Review Board Statement: Not applicable.

Informed Consent Statement: Not applicable.

Data Availability Statement: The data presented in this study are available on request from the authors.

Acknowledgments: King Mongkut's Institute of Technology Ladkrabang (KMITL), Thailand is acknowledged for fellowship granting under an academic collaborative work between KMITL and PROMES-CNRS.

Conflicts of Interest: The authors declare no conflict of interest.

References

1. Rodat, S.; Abanades, S.; Boujjat, H.; Chuayboon, S. On the path toward day and night continuous solar high temperature thermochemical processes: A review. *Renew. Sustain. Energy Rev.* **2020**, *132*, 110061. [CrossRef]
2. Boujjat, H.; Rodat, S.; Chuayboon, S.; Abanades, S. Experimental and CFD investigation of inert bed materials effects in a high-temperature conical cavity-type reactor for continuous solar-driven steam gasification of biomass. *Chem. Eng. Sci.* **2020**, *228*, 115970. [CrossRef]
3. Piatkowski, N.; Wieckert, C.; Weimer, A.W.; Steinfeld, A. Solar-driven gasification of carbonaceous feedstock—A review. *Energy Environ. Sci.* **2011**, *4*, 73–82. [CrossRef]
4. Boujjat, H.; Rodat, S.; Chuayboon, S.; Abanades, S. Experimental and numerical study of a directly irradiated hybrid solar/combustion spouted bed reactor for continuous steam gasification of biomass. *Energy* **2019**, *189*, 116118. [CrossRef]
5. Chuayboon, S.; Abanades, S.; Rodat, S. Insights into the influence of biomass feedstock type, particle size and feeding rate on thermochemical performances of a continuous solar gasification reactor. *Renew. Energy* **2019**, *130*, 360–370. [CrossRef]
6. Piatkowski, N.; Wieckert, C.; Steinfeld, A. Experimental investigation of a packed-bed solar reactor for the steam-gasification of carbonaceous feedstocks. *Fuel Process. Technol.* **2009**, *90*, 360–366. [CrossRef]
7. Gokon, N.; Izawa, T.; Kodama, T. Steam gasification of coal cokes by internally circulating fluidized-bed reactor by concentrated Xe-light radiation for solar syngas production. *Energy* **2015**, *79*, 264–272. [CrossRef]
8. Melchior, T.; Perkins, C.; Lichty, P.; Weimer, A.W.; Steinfeld, A. Solar-driven biochar gasification in a particle-flow reactor. *Chem. Eng. Process. Process. Intensif.* **2009**, *48*, 1279–1287. [CrossRef]
9. Piatkowski, N.; Steinfeld, A. Solar-Driven Coal Gasification in a Thermally Irradiated Packed-Bed Reactor. *Energy Fuels* **2008**, *22*, 2043–2052. [CrossRef]
10. Müller, F.; Poživil, P.; van Eyk, P.; Villarrazo, A.; Haueter, P.; Wieckert, C.; Nathan, G.; Steinfeld, A. A pressurized high-flux solar reactor for the efficient thermochemical gasification of carbonaceous feedstock. *Fuel* **2017**, *193*, 432–443. [CrossRef]
11. Bellouard, Q.; Abanades, S.; Rodat, S. Biomass Gasification in an Innovative Spouted-Bed Solar Reactor: Experimental Proof of Concept and Parametric Study. *Energy Fuels* **2017**, *31*, 10933–10945. [CrossRef]
12. Boujjat, H.; Rodat, S.; Chuayboon, S.; Abanades, S. Numerical simulation of reactive gas-particle flow in a solar jet spouted bed reactor for continuous biomass gasification. *Int. J. Heat Mass Transf.* **2019**, *144*, 118572. [CrossRef]
13. Chuayboon, S.; Abanades, S. An overview of solar decarbonization processes, reacting oxide materials, and thermochemical reactors for hydrogen and syngas production. *Int. J. Hydrogen Energy* **2020**, *45*, 25783–25810. [CrossRef]
14. Levêque, G.; Abanades, S. Kinetic analysis of high-temperature solid–gas reactions by an inverse method applied to ZnO and SnO_2 solar thermal dissociation. *Chem. Eng. J.* **2013**, *217*, 139–149. [CrossRef]
15. Chuayboon, S.; Abanades, S.; Rodat, S. Solar chemical looping gasification of biomass with the ZnO/Zn redox system for syngas and zinc production in a continuously-fed solar reactor. *Fuel* **2018**, *215*, 66–79. [CrossRef]
16. Chambon, M.; Abanades, S.; Flamant, G. Solar thermal reduction of ZnO and SnO_2: Characterization of the recombination reaction with O_2. *Chem. Eng. Sci.* **2010**, *65*, 3671–3680. [CrossRef]
17. Chambon, M.; Abanades, S.; Flamant, G. Design of a Lab-Scale Rotary Cavity-Type Solar Reactor for Continuous Thermal Dissociation of Volatile Oxides under Reduced Pressure. *J. Sol. Energy Eng.* **2010**, *132*, 021006. [CrossRef]
18. Abanades, S. CO_2 and H_2O reduction by solar thermochemical looping using SnO_2/SnO redox reactions: Thermogravimetric analysis. *Int. J. Hydrogen Energy* **2012**, *37*, 8223–8231. [CrossRef]
19. Abanades, S. Thermogravimetry Analysis of CO_2 and H_2O Reduction from Solar Nanosized Zn Powder for Thermochemical Fuel Production. *Ind. Eng. Chem. Res.* **2011**, *51*, 741–750. [CrossRef]
20. Boujjat, H.; Rodat, S.; Chuayboon, S.; Abanades, S. Combustion-assisted solar gasification of biomass particles in a high temperature conical jet spouted bed reactor. *AIP Conf. Proc.* **2020**, *2303*, 170002. [CrossRef]
21. Abanades, S.; Rodat, S.; Boujjat, H. Solar Thermochemical Green Fuels Production: A Review of Biomass Pyro-Gasification, Solar Reactor Concepts and Modelling Methods. *Energies* **2021**, *14*, 1494. [CrossRef]
22. Boujjat, H.; Rodat, S.; Abanades, S. Techno-Economic Assessment of Solar-Driven Steam Gasification of Biomass for Large-Scale Hydrogen Production. *Processes* **2021**, *9*, 462. [CrossRef]
23. Bellouard, Q.; Rodat, S.; Grateau, M.; Abanades, S. Solar Biomass Gasification Combined with Iron Oxide Reduction for Syngas Production and Green Iron Metallurgy. *Front. Energy Res.* **2020**, *8*, 66. [CrossRef]
24. Yang, J.; Wei, Y.; Yang, J.; Xiang, H.; Ma, L.; Zhang, W.; Wang, L.; Peng, Y.; Liu, H. Syngas production by chemical looping gasification using Fe supported on phosphogypsum compound oxygen carrier. *Energy* **2019**, *168*, 126–135. [CrossRef]
25. Xue, N.; Wang, Z.; Wu, J.; He, T.; Zhang, J.; Li, J.; Wu, J. Effect of equivalence ratio on the CO selectivity of Fe/Ca-based oxygen carriers in biomass char chemical looping gasification. *Fuel* **2019**, *252*, 220–227. [CrossRef]
26. Kruesi, M.; Jovanovic, Z.R.; Haselbacher, A.; Steinfeld, A. Analysis of solar-driven gasification of biochar trickling through an interconnected porous structure. *AIChE J.* **2014**, *61*, 867–879. [CrossRef]
27. Chuayboon, S.; Abanades, S.; Rodat, S. Comprehensive performance assessment of a continuous solar-driven biomass gasifier. *Fuel Process. Technol.* **2018**, *182*, 1–14. [CrossRef]
28. Bellouard, Q.; Abanades, S.; Rodat, S.; Dupassieux, N. Solar thermochemical gasification of wood biomass for syngas production in a high-temperature continuously-fed tubular reactor. *Int. J. Hydrogen Energy* **2017**, *42*, 13486–13497. [CrossRef]

29. Chuayboon, S.; Abanades, S.; Rodat, S. Experimental analysis of continuous steam gasification of wood biomass for syngas production in a high-temperature particle-fed solar reactor. *Chem. Eng. Process. Process. Intensif.* **2018**, *125*, 253–265. [CrossRef]